ELECTROMAGNETIC SYNTHESIS OF OVERLAP-GAP-COUPLED MICROSTRIP FILTERS †

Owen Fordham, Ming-Ju Tsai, and Nicolaos G. Alexopoulos

Electrical Engineering Department, University of California, Los Angeles, CA 90024

† This research was supported by U. S. Army Research Grant DAAH 04-93-G-0228.

Abstract

This paper presents a technique for electromagnetic synthesis of microstrip overlap-gap-coupled filters. The algorithm uses a rigorous analysis, which solves an electric field integral equation in the spectral domain using the method of moments, inside an outer loop that optimizes the filter dimensions. A piecewise synthesis procedure generates initial dimensions that provide a good starting point for direct electromagnetic optimization of the complete filter. Measured results for a five-section filter are shown that verify the accuracy of this design method.

I. Introduction

Many computer programs have been developed that perform rigorous electromagnetic (EM) analysis of microwave printed circuits using the method of moments (MoM), some of which are general enough to handle geometries that involve multiple conductors and/or multiple dielectric layers. These programs are good analysis tools, but they do not provide synthesis capability. In the case of filter design, the designer must iteratively tune the dimensions based on the computed response. A skilled designer may arrive at the optimum filter geometry, but since each analysis run is time consuming (typically hours on a modern work-station), this process may not be any faster than the traditional empirical approach in the laboratory. One novel solution to this dilemma is the "space mapping" technique developed by Bandler, et. al. [1].

We are presenting an algorithm and code developed to synthesize microstrip overlap-gap-coupled filters. Our approach emphasizes direct EM optimization, rather than conventional filter synthesis technique, and takes advantage of specific features of the structure to accelerate computation. This filter structure is formed by alternating half-wave open-circuit resonators between the interface and the top of two dielectric layers (see Figure 1), and controlling the couplings by adjusting the amount of overlap [2]. In comparison to conventional microstrip filter designs that use half-wave open-circuit resonators, the overlaps allow higher coupling between resonators with lower sensitivity to etching tolerances; therefore, broader bandwidth filters can be realized.

To synthesize this filter, computer code which performs rigorous EM analysis was placed inside an outer loop that optimizes the filter dimensions to achieve the prescribed response. The analysis applies the method of moments in the spectral domain to solve an electric field integral equation. Since the analysis can predict all the EM interactions between resonators and feed lines (such as coupling between non-adjacent resonators due to surface waves or radiation), these effects can be compensated for during optimization.

Synthesized and measured results for a five-section design example are compared in this paper. An open structure was chosen for this example to allow convenient fabrication and measurement. In practice, printed circuit filters are enclosed, when possible, to improve out-of-band rejection. The program has the capability to synthesize filters that are either open or covered, and with or without sidewalls.

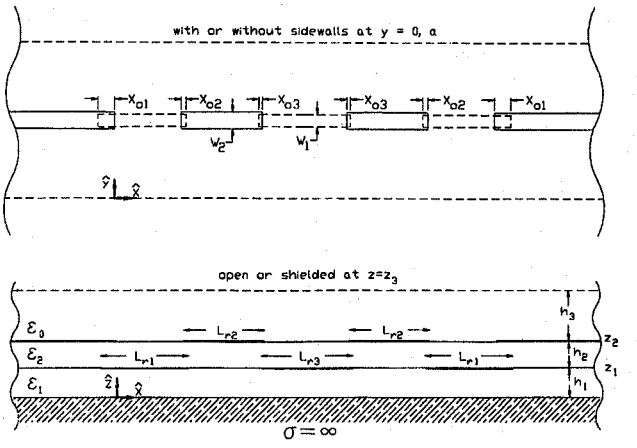

Figure 1. Overlap-gap-coupled filter geometry.

II. Analysis Method

The Green's function for microstrip with two dielectric layers is conveniently derived in the spectral domain. The Fourier transform with respect to the transverse (y) coordinate is either finite or infinite, depending on whether or not perfectly conducting sidewalls are present [3]. With sidewalls located at $y = 0$ and $y = a$, the spectral variable λ_y becomes limited to the discreet values $\lambda_{ym} = n\pi/a$, where n is odd. The

choice of a structure that is open or covered at $z = z_3$ (by a perfectly conducting plane) is allowed by conditionally altering a term in the transformed Green's function.

Filter responses must be computed many times during optimization of the filter dimensions, so assumptions concerning the unknown current distribution are made to increase computation speed. The conducting strips are considered to be infinitesimal in thickness, perfectly conducting, and located at either the dielectric interface (z_1) or the top (z_2) (see Figure 1). The transverse distribution of current on each strip in the filter is assumed to be identical to the corresponding infinite line case. Prior to synthesizing the filter, a single infinite line is analyzed for each combination of strip width and height that will occur in the resonators and feed lines. The transverse distributions of current components $J_x(y)$ and $J_y(y)$ are expanded with a cosine and sine series, respectively, multiplied by a Maxwell function to satisfy the edge condition. Accurate solutions are obtained with only a few terms of the series. Piece-wise sinusoidal (PWS) functions [4] are used to expand the longitudinal (x) distribution of current on the resonators. Current on the input and output feeding lines is represented by travelling wave modes (TWMs) [5] that are modified to force the current to zero at the open ends. Their main advantage is that their weights are the reflection and transmission coefficients, when a weight of unity is assumed for the incident travelling wave mode. The propagation constants for these TWM functions is obtained from the infinite line analyses described previously. PWS functions are superposed on the feed lines to allow the method of moments to solve for arbitrary current distributions near the open ends.

The reaction (inner product) of E_x with the x component of each individual basis function is set to zero, and enforced in the transformed domain. The procedure is nearly Galerkin, except that two extra PWS testing functions are substituted for the TWM functions to avoid convergence problems. For a total of N PWS basis functions, a linear system $\boldsymbol{Z}\,\boldsymbol{I}=\boldsymbol{V}$ of N+2 equations results. The unknown vector $\boldsymbol{I}$ consists of the weights of the PWS basis functions along with Γ and T. For $m \le N+2$ and $n \le N$, the matrix element Z_{mn} represents the transformed reaction between the mth PWS testing function and the electric field produced by the nth PWS basis function:

$$Z_{m,n} = \int_{-\infty}^{\infty} \frac{4\,\alpha_k \alpha_l e^{j[\lambda_x(x_m - x_n)]}}{\sin(\alpha_k d_m)\,\sin(\alpha_l d_n)} \left[\frac{\cos(\alpha_k d_m) - \cos(\lambda_x d_m)}{\lambda_x^2 - \alpha_k^2}\right] \left[\frac{\cos(\alpha_l d_n) - \cos(\lambda_x d_n)}{\lambda_x^2 - \alpha_l^2}\right] F_{kl}(\lambda_x)\, d\lambda_x \tag{1}$$

where x_m and d_m are the testing function's x coordinate and size, k is a layer index indicating the testing function's layer location ($z = z_k$, k = 1 or 2); x_n, d_n, and l are for the basis function; $\alpha_k, \alpha_l = \kappa_0[(\epsilon_{r1}+\epsilon_{r2})/2]^{1/2}$ or $\kappa_0[(\epsilon_{r2}+1)/2]^{1/2}$ for k, l =1 or 2 respectively; $F_{kl}(\lambda_x)$ is the result of integration or summation with respect to λ_y, defined in (3) and (4). The last two columns of $\boldsymbol{Z}$ and the vector $\boldsymbol{V}$ represent the transformed reactions between PWS functions and the reflected, transmitted, and incident TWM basis functions. For example, the $Z_{m,N+1}$ element is the reaction between the mth PWS testing function and the reflected TWM basis function:

$$Z_{m,N+1} = \int_{-\infty}^{\infty} \frac{2\,\alpha_k e^{jx_m\lambda_x}}{\sin(\alpha_k d_m)} \left[\frac{\cos(\alpha_k d_m) - \cos(\lambda_x d_m)}{\lambda_x^2 - \alpha_k^2}\right] \left[\frac{-(1+j)\beta + j\sqrt{2}\,\beta\, e^{-jx_p\lambda_x} + (\lambda_x + \beta)e^{-jx_t\lambda_x}}{j(\lambda_x^2 - \beta^2)}\right] F_{kl}(\lambda_x)\, d\lambda_x \tag{2}$$

where the input line is anchored at $x = 0$, and β is its propagation constant; x_p is $\frac{1}{8}\lambda_g$ from the open end, where the real part (cosine term) of the TWM is truncated and pieced together with a real sine term to force the current to zero at the open end [6]; x_t is several λ_g away from the open end, where the TWM is truncated to remove the singularity from its transform [6], and represents termination of the strip's reflected current in a matched source resistance.

For the open structure, the transformed reaction with respect to λ_y is given by

$$F_{kl}(\lambda_x) = \int_{-\infty}^{\infty} \left[\, \tilde{G}_{xx}^{kl}(\lambda_x, \lambda_y)\, \tilde{J}_x^{l}(\lambda_y)\, \tilde{J}_x^{k*}(\lambda_y) + \tilde{G}_{xy}^{kl}(\lambda_x, \lambda_y)\, \tilde{J}_y^{l}(\lambda_y)\, \tilde{J}_x^{k*}(\lambda_y) \,\right] d\lambda_y \tag{3}$$

where ~ denotes a Fourier transformed quantity; G_{xx} and G_{xy} are components of the dyadic Green's function; $J_x(y)$ and $J_y(y)$ are the transverse distributions of x and y currents. Both the λ_x and λ_y contours of integration are deflected off the real axis in a triangular shape to avoid the surface wave pole(s) and branch points [7]. Tail integrals are efficiently and accurately computed by separating exp(+jλ), exp(-jλ), and non-oscillating dependencies, and following the appropriate contours to eliminate the oscillations.

In the presence of sidewalls, the reaction with respect to λ_y is evaluated with the following summation:

$$F_{kl}(\lambda_x) = \sum_{\substack{n=1 \\ n\ \text{odd}}}^{\infty} \left[\, \tilde{G}_{xx}^{kl}(\lambda_x, \frac{n\pi}{a})\, \tilde{J}_x^{l}(\frac{n\pi}{a})\, \tilde{J}_x^{k*}(\frac{n\pi}{a}) + \tilde{G}_{xy}^{kl}(\lambda_x, \frac{n\pi}{a})\, \tilde{J}_y^{l}(\frac{n\pi}{a})\, \tilde{J}_x^{k*}(\frac{n\pi}{a}) \,\right] \tag{4}$$

An accelerating series is used to extract the n^{-2} asymptotic behavior, which vastly improves convergence.

Rectangular coordinates in λ are advantageous because the result of integration or summation with respect to λ_y is independent of the x geometry and constant for all pairs of basis functions which have the same combination of strip widths and heights. The same contour in λ_x is maintained for the evaluation of every Z_{mn}, so that $F_{kl}(\lambda_x)$ can be computed once at sample points along the contour and stored in a database [7]. Then for each Z_{mn}, quadratic interpolation of the database returns $F_{kl}(\lambda_x)$ during the numerical integration with respect to λ_x. The same database is valid throughout optimization of the filter's resonator lengths and overlaps, since the filter is collinear.

The individual matrix elements are reactions between current elements (single PWS basis functions) that are small compared to wavelength, so they vary slowly and smoothly with frequency, in contrast to the linear system's solution [6]. Therefore, to reduce computation time, the matrix elements are computed at a set of frequencies spaced too far apart to capture details of the filter's frequency response. The response is filled in by solving the linear system using matrix elements that are interpolated from the original set.

III. Synthesis Algorithm

Filter synthesis proceeds from a single execution command, with the dielectric layers and strip widths given as inputs. Infinite line analyses are done for each unique strip width and location (interface or top) in the filter to yield $J_x(y)$ and $J_y(y)$. The λ_x contour is defined and the databases in $F_{11}(\lambda_x)$, $F_{12}(\lambda_x)$, and $F_{22}(\lambda_x)$ are computed. The algorithm then generates initial filter dimensions (resonator and overlap lengths) using a piecewise synthesis method described below.

A series-capacitor-coupled, transmission line filter with half-wave open circuit resonators provides a first-order model of the overlap-gap-coupled microstrip filter. Since the response of the model can be computed much faster than the response of the real filter, these capacitor values and line lengths are optimized using the same routines which will be used later to optimize the real filter. Next, an overlap length in two-layer microstrip is found that produces the same $|T|$ as each coupling capacitor in the model filter [8]. Numerical searches then find doubly-loaded resonator lengths that correspond to each pair of overlaps. These dimensions provide the starting point for EM optimization of the complete filter.

Many PWS basis functions per resonator are required to accurately analyze overlap-gap filters. With a large reaction matrix, direct computation of the frequency response is so slow that it can not be placed inside an optimization loop. Instead, most of the reactions are determined by interpolating a large reaction database, created prior to optimization. The time to compute a single frequency response is still significant, even though it has been drastically reduced by interpolating the reaction database. Consequently, a minimization scheme that uses very few error function evaluations is desirable. The derivatives of the error function (with respect to the filter dimensions) are not available. Given these considerations, a modified version of Powell's method was chosen to perform the multi-dimensional minimization.

IV. Results and Measurements

An open overlap-gap-coupled microstrip filter with five sections was synthesized to yield 0.1 dB ripple across 31 percent bandwidth at 10 GHz, Chebychev low-side rejection, and relaxed high side rejection. Given input parameters of ϵ_{r1}= 2.2, ϵ_{r2}= 9.8, h_1= 0.010", h_2= 0.010", w_1= 0.018", and w_2= 0.032", the program converged to the following optimum dimensions: x_{o1}= 0.0516", x_{o2}= 0.0152", x_{o3}= 0.0106", l_{r1}= 0.2752", l_{r2}= 0.2542", and l_{r3}= 0.2851".

To fabricate the filter, a top layer of alumina, clad with thin (0.3 mil) layers of conductor, was etched on both sides to form the resonators and the input and output lines. The finite strip thickness apparently caused a small (0.3 mil) air gap at the duroid/alumina interface, despite an attempt to eliminate it by deforming the soft duroid with pressure applied from the top. A pair of two-layer microstrip-to-coaxial transitions was fabricated and characterized with the line-reflect-line (LRL) method. Deembedding removed the degrading effect of the transitions from raw measurements of the filter.

Figure 2 compares the synthesized filter response to the measured response. With no tuning, the measured low side rejection, passband VSWR, upper stopband, and second passband are all in good agreement with the theory.

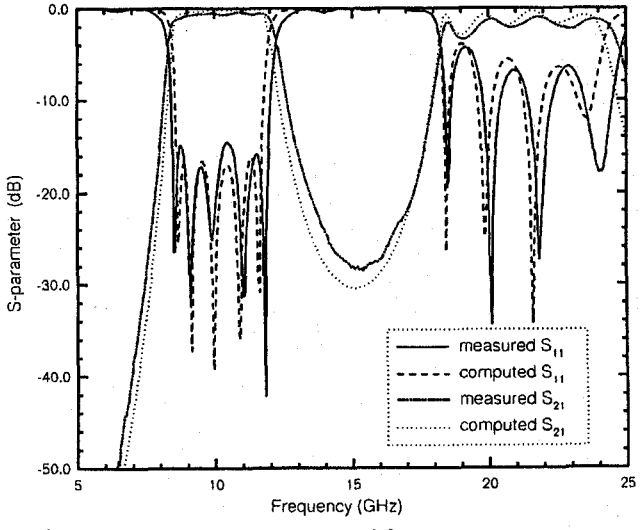

Figure 2. Measured vs. computed frequency response.

However, the measured bandwidth is 370 MHz wider than predicted. We suspected that the primary source of error was deviation of the filter's $J_x(y)$ and $J_y(y)$ from the infinite lines'

$J_x(y)$ and $J_y(y)$. To check this possibility, the fabricated dimensions were entered into a full-wave analysis program that models printed circuits of arbitrary shape [9]. This program solves a mixed potential integral equation in the spatial domain using the method of moments with triangular subdomain basis functions. The computed bandwidth and VSWR pattern matched the measurement quite well, but the computed center frequency was 250 MHz low. Since the accuracy of this program had already been verified (by comparison to measurements of a variety of printed circuits), we investigated the possibility that the small air gap caused by the finite metallization thickness of the resonators at the interface had shifted the fabricated filter's center frequency.

Static 2-D finite-element analyses showed that a $\Delta\epsilon_{r1} = -0.11$ would produce the same propagation constant as a cross-section with 0.3 mil air layer at the substrate interface due to the 0.3 mil strip thickness. The filter was analyzed again with the full-wave program, using the low end of the tolerance for each dielectric constant ($\epsilon_{r1} = 2.18$ and $\epsilon_{r2} = 9.6$) and an additional $\Delta\epsilon_{r1} = -0.11$ to absorb the effect of the air gap. These modified dielectric constants produced excellent agreement between the measurement and full-wave theory, shown in Figure 3. Also compared is the approximate analysis used for filter synthesis, run using the modified dielectric constants. The approximation concerning $J_x(y)$ and $J_y(y)$ appears to shift the lower band edge up by 200 MHz.

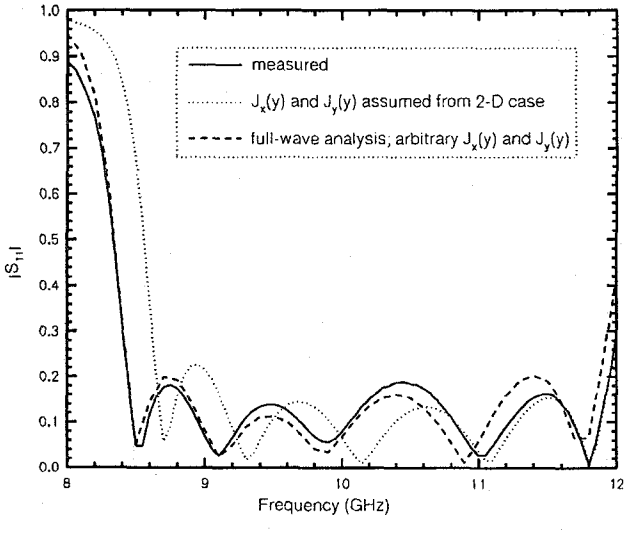

Figure 3. Filter response computed with modified dielectric constants (ϵ_{r1}=2.07 and ϵ_{r2}=9.6) and fabricated dimensions.

V. Conclusions

To demonstrate the EM synthesis technique, a five-section overlap-gap-coupled filter was designed in a single automated computer run. After fabrication and without tuning, good agreement between measured and synthesized frequency responses was observed. We have shown that the small discrepancy in bandwidth will be resolved by solving for an arbitrary $J_x(y)$ and $J_y(y)$ during filter optimization. This capability is being implemented.

In the design example, the piece-wise synthesis to produce initial dimensions resulted in a frequency response that was already close to the goal; direct EM optimization of the complete filter only fine-tuned the response. However, the need for EM synthesis will be emphasized by a cross-coupled version of this filter, which we are developing. The cross-coupling(s) will place a transmission zero(s) to improve upper-side rejection, and will be sensitive to EM interactions between non-adjacent resonators and feed lines, making it imperative to analyze the complete filter during synthesis.

VI. Acknowledgements

Owen Fordham extends his appreciation to Hughes Aircraft Co. for the support of a Hughes Doctoral Fellowship.

VII. References

[1] J. W. Bandler, R. M. Biernacki, S. H. Chen, P. A. Grobelny, and R. H. Hemmers, "Space mapping technique for electromagnetic optimization," *IEEE Trans. Microwave Theory Tech.*, vol. MTT-42, pp.2536–2543, Dec. 1994.

[2] H. Y. Yang and N. G. Alexopoulos , "Basic blocks for high-frequency interconnects: theory and experiment," *IEEE Trans. Microwave Theory Tech.*, vol. MTT-36, pp.1258–1264, Aug. 1988.

[3] T. Itoh, *Numerical Techniques for Microwave and Millimeter-Wave Passive Structures*. New York, NY: John Wiley & Sons, 1989.

[4] P. B. Katehi and N. G. Alexopoulos, "On the modelling of electromagnetically coupled microstrip antennas—the printed strip dipole," *IEEE Trans. Antennas Propagat.*, vol. AP-32, pp.1179–1186, Nov. 1984.

[5] R. W. Jackson and D. M. Pozar, "Full-wave analysis of microstrip open-end and gap discontinuities," *IEEE Trans. Microwave Theory Tech.*, vol. MTT–33, pp.1036-1042, Oct. 1985.

[6] H. Y. Yang, private communication.

[7] H. Y. Yang, A. Nakatani, and J. Castañeda, "Efficient evaluation of spectral integrals in the moment method solution of microstrip antennas and circuits," *IEEE Trans. Antennas Propagat.*, vol. AP-38, pp. 1127–1129, July 1990.

[8] W. Schwab, F. Bogelsack, and W. Menzel, "Multilayer suspended stripline and coplanar line filters," *IEEE Trans. Microwave Theory Tech.*, vol. MTT-42, pp.1403–1407, July 1994.

[9] M. J. Tsai and N. G. Alexopoulos, "Proximity coupled filter elements and interconnects of arbitrary shape in multilayered media," accepted for publication in *IEEE MTT-S Int. Microwave Symp. Dig.*, 1995.